Abundances of UV bright stars in globular clusters. I. ROA 5701 in ω Centauri and Barnard 29 in M 13 [*]

S. Moehler, U. Heber, M. Lemke, and R. Napiwotzki

Dr. Remeis-Sternwarte, Astronomisches Institut der Universität Erlangen-Nürnberg, Sternwartstr. 7, 96049 Bamberg, Germany

Abstract. Two UV brights stars in globular clusters, *ROA 5701* (ω Cen) and *Barnard 29* (M 13) are analysed from high-resolution UV and optical spectra. The main aim is the measurement of iron abundances from UV spectra obtained with the HST-GHRS. In addition atmospheric parameters and abundances for He, C, N, O, and Si are derived from optical spectra (ESO CASPEC) for *ROA 5701* or taken from literature for *Barnard 29*. Both stars are found to be post-asymptotic giant branch stars. Surprisingly, their iron abundances lie significantly below the cluster abundance in both cases. *Barnard 29* lies 0.5 dex below the iron abundance derived for giant stars in M 13 and the iron abundance of *ROA 5701* is the lowest of any star in ω Cen analysed so far. *Barnard 29* shows the same abundance pattern as the red giant stars in M 13, except for its stronger iron deficiency. The iron depletion could be explained by gas-dust separation in the AGB progenitor's atmosphere, if iron condensed into dust grains which were then removed from the atmosphere by a radiatively driven wind. The interpretation of the abundance pattern for *ROA 5701* is hampered by the star-to-star abundance variations seen in ω Cen, but its abundance pattern appears to be consistent with the gas-dust separation scenario.

1. Introduction

The term "UV bright stars" was introduced by Zinn et al. (1972) for stars in globular clusters that lie above the horizontal branch (HB) and are bluer than red giants. The name resulted from the fact that in the U band these stars were brighter than all other cluster stars. Further investigations showed that this group of stars consists of post-AGB stars, evolving away from the asymptotic giant branch (AGB) to the white dwarf domain (Sweigart et al., 1974; de Boer 1987), and of so-called Supra-HB stars that evolve from the blue HB (BHB) towards higher luminosities (Dorman et al., 1993) but do not have enough mass to ascend the AGB. Both evolutionary stages are immediate precursors to white dwarfs.

Up to now detailed analyses have been performed mainly for post-AGB stars in the field of the Milky Way (McCausland et al., 1992; Napiwotzki et al. 1994), for which the population membership is difficult to establish. The summarized result of these analyses is that the abundances of N, O, and Si are roughly 1/10 of the solar values, while Fe and C are closer to 1/100 solar. McCausland et al. (1992) and Conlon (1994) interpret the observed abundances as the results of dredge-up processes on the AGB, i.e. the mixing of processed material from the stellar interior to the surface. Although this hypothesis contradicts stellar evolution theories (Renzini & Voli 1981; Iben & Renzini 1984; Vassiliadis & Wood 1993), which do not predict any dredge-up processes for the low-mass precursors of these objects, compelling evidence that such dredge-up processes do occur is provided by K 648, the central star of the Planetary Nebula Ps 1 in M 15. Its atmosphere is strongly enriched in carbon when compared to the cluster carbon abundance (Heber et al., 1993) pinpointing the dredge-up of triple α processed material to the stellar surface.

Napiwotzki et al. (1994) discuss another possible explanation: The photospheric abundances of the Pop II central star BD+33°2642 (and also of the objects analysed by McCausland et al., 1992) can be understood as the results of gas-dust separation towards the end of the AGB phase, which leads to a depletion of certain elements. This process has already been proposed by Bond (1991) for some cooler post-AGB stars with extreme metal deficiencies. A

distinction between the two scenarios is hampered by the fact that the original metallicities remain unknown. Iron is one of the elements which are most sensitive to depletion. Thus the knowledge of its abundance in the UV bright stars and a comparison with the known cluster metallicity allows an unambiguous distinction between both scenarios. Unfortunately, for hot metal poor stars iron is not accessible for a spectroscopic analysis from optical spectra due to the lack of lines in this wavelength region. In the ultraviolet, however, a large number of spectral lines can be used. Hence the Goddard High Resolution Spectrograph (GHRS) of the Hubble Space Telescope was used to measure the iron line spectra of *ROA 5701* and *Barnard 29*.

2. Observations and data reduction

2.1. UV spectroscopy

The UV spectra of *ROA 5701* and *Barnard 29* were obtained with the Goddard High Resolution Spectrograph onboard the Hubble Space Telescope, equipped with the G200M grating ($1860 - 1906$ Å, 0.07 Å resolution) and using the large science aperture. This spectral region was chosen because the strongest Fe III absorption lines are expected there as judged from the high resolution IUE spectra of BD+33°2642 (Napiwotzki et al., 1994), which shows an optical spectrum similar to *ROA 5701* and *Barnard 29*. The exposure times were 4711 s for *ROA 5701* (observed on August 3rd, 1996) and 4570 s for *Barnard 29* (observed on November 30th, 1996). We did not use the FP split option as we did not expect any lines strong enough to allow a correct alignment of the individual spectra by correlation.

After the standard pipeline reduction we co-added the flux of the individual spectra, which were on identical wavelength scales. The resulting spectra were converted to MIDAS bdf-format and interpolated to a step size of 0.02 Å. They were then corrected for Doppler shifts using the heliocentric radial velocities of the clusters (+232 km/sec, ω Cen; -246 km/sec, M 13) and the corrections for heliocentric velocities appropriate for the observation dates. To allow a better definition of the continuum we smoothed the spectra with a 3 pixel wide box average filter. The continuum was then defined by eye and we estimate that the error of the normalization lies between 5% and 10%.

Fig. 1 shows a section of the GHRS spectra of *ROA 5701* and *Barnard 29* compared to the IUE data of BD+33°2642[1], a field post-AGB star with T_{eff} and $\log g$ similar to *ROA 5701* and *Barnard 29*. The abundance noted for BD+33°2642 in Fig. 1 was derived from equivalent width measurements (Napiwotzki et al., 1994) for a microturbulent velocity of 10 km/s (which is the

value Conlon et al., 1994, derived for *Barnard 29*.) The iron abundance of BD+33°2642 is comparable to that of M 13 and ω Cen. The much weaker iron lines in the GHRS spectra therefore suggest that *Barnard 29* and *ROA 5701* show significant iron depletions.
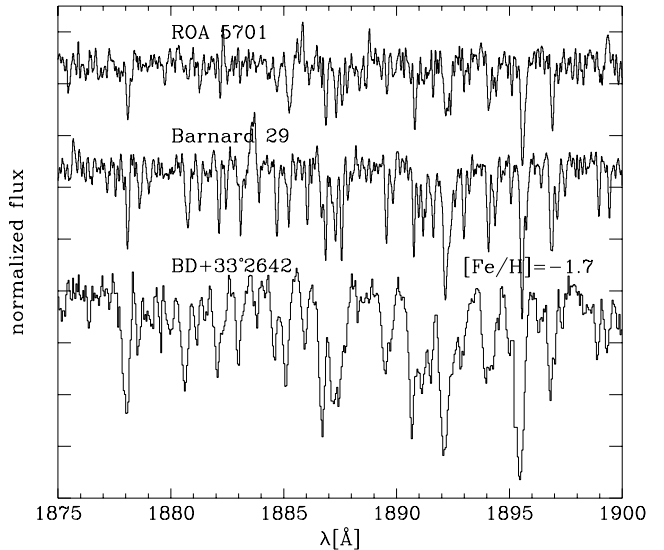
Fig. 1. The GHRS spectra of *ROA 5701* and *Barnard 29*, compared to IUE high resolution spectra of BD+33°2642[1]. The GHRS data were smoothed by convolution with a Gaussian of 0.06 Å FWHM, which yields a "smoothed" resolution of 0.09 Å, similar to that of the IUE data (0.1 Å). We used a microturbulent velocity of 10 km/s to derive the abundance noted for BD+33°2642.

2.2. Optical high resolution spectra

ROA 5701 was observed with the ESO CAssegrain echelle SPECtrograph (CASPEC) at the 3.6m telescope at La Silla, Chile, on May 24, 1988. Two spectra of 1 hour integration time each were obtained. The spectra were binned during read out in order to improve the S/N ratio. Reduction of the data proceeded in two steps: first the ESO-MIDAS software (Ponz & Brinks, 1986) in Garching was used for wavelength calibration and extraction of the echelle orders. The background correction and flat fielding were done separately using a computer program written by G. Jonas (Kiel, see Heber et al., 1988). We then merged the orders of the CASPEC spectra and rebinned them to a common wavelength scale. The spectra have a resolution of 0.3 Å.

2.3. Equivalent widths

We always used the normalized spectra to measure equivalent widths. The measurement in the optical spectra was straightforward since the lines are isolated and well defined and the spectra have a good S/N. In the UV, however, the lines are more crowded and the S/N is lower. Therefore,

---

[1]   For this purpose the IUE spectra SWP04791, SWP37966, SWP43623, SWP45533 were calibrated with the NEWSIPS software and co-added

three different methods were used: i) direct integration without any fit of the line shape using a global continuum (assuming that the overall continuum definition is more reliable than a local one due to the low S/N), ii) same as i), but for a local continuum, and iii) fitting Gaussians to the absorption line profiles (using a locally defined continuum). Method iii) could not be used for *ROA 5701* because the lines were too weak.

For the GHRS data the equivalent widths measured for a global continuum (which were used for the abundance determinations) were on average larger than those measured for a locally defined continuum. This offset leads to a difference in the mean iron abundance of 0.08 dex for *ROA 5701* and 0.03 dex for *Barnard 29*.

For the CASPEC data the equivalent widths measured for a global continuum resulted in abundances larger than those determined for a local continuum by 0.12 dex for O, 0.02 dex for N, and 0.14 dex for Si. As the CASPEC spectra showed small-scale continuum variations that are difficult to correct for by a global continuum fit we decided to keep the abundances derived from the "local continuum" equivalent widths.

3. Effective temperatures, gravities and helium abundances

Detailed analyses of optical spectra are available for *Barnard 29* (Conlon et al., 1994), whereas only an estimate of the effective temperature from low resolution IUE spectra (Cacciari et al., 1984, $T_{eff} = 24000$ K, $E_{B-V} \geq 0^m11$) exists for *ROA 5701*. Therefore we determined the photospheric parameters of *ROA 5701* by analysing the optical CASPEC spectra together with optical photometry (Norris 1974) and low resolution IUE spectrophotometry (SWP07849, LWR06845).

To derive a first estimate of the temperature we dereddened the optical photometry and the IUE data, using the interstellar extinction law of Savage & Mathis (1979). The UBV magnitudes were converted into fluxes, using the conversion given by Heber et al. (1984). The data were then fitted with ATLAS9 (Kurucz 1992) models for [M/H] $= -1.5$. For a reddening of 0^m11 (Norris, 1974) resp. 0^m15 (Djorgovski, 1993) the best fits were achieved for effective temperatures of 22000 K resp. 24000 K. These results compare very well to those of Cacciari et al. (1984).

For the temperatures given above we fitted ATLAS9 model spectra with solar helium abundances and [M/H] $= -1.5$ to the Balmer lines and obtained the surface gravities from the best fit. To verify our results we also derived effective temperature, surface gravity, and helium abundances from the Balmer and He I line profiles only. For this purpose we calculated model atmospheres using ATLAS9 (Kurucz 1991, priv. comm.) and used the LINFOR spectrum synthesis program (developed originally by Holweger, Steffen, and Steenbock at Kiel university) to compute a grid of theoretical spectra, which include the

Balmer lines H_α to H_{22} and He I lines. The grid covered the range $10000 \ldots 27500$ K in T_{eff}, $2.5 \ldots 5.0$ in $\log g$ and $-2.0 \ldots -0.3$ in $\log \frac{N_{He}}{N_H}$ at a metallicity of -1. For the actual fit we used the routines developed by Bergeron et al. (1992) and Saffer et al. (1994), which employ a χ^2 test. The results of all procedures are listed in Table 1. It is clear that the agreement is rather good. For the further analysis we used the mean value of the IUE derived results, i.e. an effective temperature of 23000 K and a log g value of 3.3.

4. Abundance analysis

The determination of elemental abundances is interlocked with the microturbulent velocity ξ, which can be derived if a sufficient number of lines of one ion can be measured over a wide range of line strengths. In the optical O II lines are most suitable for this purpose as they are most frequent. For *ROA 5701* we could measure equivalent widths of 22 O II lines, which yield a value of 20 km/s for ξ. Gies & Lambert (1992) note in their analysis of B-type supergiants that the high microturbulent velocities of about 20 km/s obtained from LTE analyses decrease to about 10 km/s if NLTE effects are taken into account. The microturbulent velocity of *Barnard 29*, $\xi=10$ km/s, has been determined by Conlon et al. (1994). [2]

4.1. Methods

Abundances have been derived using the classical curve-of-growth technique as well as a spectrum synthesis technique. In both cases we computed model atmospheres for the appropriate values of effective temperature, surface gravity, and cluster metallicity and used the LINFOR spectrum synthesis package for the further analysis.

curve of growth analysis We calculated curves of growth for the elements of interest, from which abundances were derived. We took into account that in many cases more than one line contributed to the measured equivalent widths by treating those lines as blends in LINFOR. In addition we tried to avoid lines with significant contributions from other elements or ions.

spectrum synthesis In a second trial we fitted the whole spectrum at once. In this mode the LINFOR package tries to fit the line profiles of the metal lines using a χ^2 test by adjusting the abundance of the element(s) that are fitted. We used the same line lists as for the curve-of-growth analysis.

---

[2] If we exclude the blend at $\lambda\lambda$ 1892.3 Å from the line list the Fe III lines yield 10 km/s for ξ for *Barnard 29*. For *ROA 5701* we derive a microturbulent velocity of 2–3 km/s from the measured Fe III lines. Determinations of ξ from model spectra to which noise was added show that noise tends to increase the measured microturbulent velocity rather than decrease it.

Table 1. Photospheric parameters of our programme stars.

Name	$T_{\rm eff}$ [K]	log g	$\log \frac{N_{\rm He}}{N_{\rm H}}$	remarks
ROA 5701	22000	3.2	−1.00	$E_{B-V}= 0.^{\rm m}11$, [M/H] = −1.5, fixed He abundance
ROA 5701	24000	3.4	−1.00	$E_{B-V}= 0.^{\rm m}15$, [M/H] = −1.5, fixed He abundance
ROA 5701	24500	3.4	−0.98	Balmer and He I line profiles only, [M/H] = −1.0
Barnard 29	20000	3.0	−1.06	Conlon et al., 1994, [M/H] = −1.0

Table 2. Equivalent widths and abundances for C II (upper limit only), N II, O II, and Si III as derived from the CASPEC spectra of *ROA 5701*.

Ion/ Multiplet	λ [Å]	χ [eV]	log gf	W_λ [mÅ]	$\log \epsilon$
C II 6	4267.020⌉	18.047	0.559		
6	4267.270⌋	18.047	0.734	<10	<5.78
N II 12	3995.000	18.498	0.225	38	6.79
15	4447.030[1]	20.411	0.238	20	6.86
O II 17	3919.285	25.655	-0.247	36	8.29
10	4069.623⌉	25.625	0.157		
10	4069.886⌋	25.632	0.365	86	7.98
10	4075.862	25.658	0.700	66	7.73
48	4089.285	28.699	0.885	59	8.22
20	4119.216	25.842	0.454	33	7.63
36	4189.600⌉	28.354	-0.821		
36	4189.789⌋	28.354	0.723	35	7.99
59	4302.858⌉	31.311	0.092		
59	4303.070⌉	31.311	-0.008		
2	4303.836⌋	28.814	0.660	37	8.17
2	4345.559	22.973	-0.330	36	7.80
2	4349.426	22.993	0.085	54	7.62
2	4366.888	22.993	-0.319	38	7.82
5	4414.901	23.435	0.211	71	7.79
5	4416.973	23.413	-0.041	54	7.86
32	4447.673[1]⌉	28.354	-1.380		
32	4448.186[1]⌋	28.354	0.047	20	7.79
14	4590.972	25.655	0.346	53	8.06
14	4595.960⌉	25.655	-1.037		
14	4596.176⌋	25.655	0.196	41	8.03
1	4638.857	22.960	-0.307	41	7.90
1	4641.817	22.973	0.084	78	7.91
1	4649.143	22.993	0.343	112	7.93
1	4650.842	22.960	-0.331	45	7.97
1	4661.633	22.973	-0.249	61	8.08
1	4676.236	22.993	-0.359	41	7.96
35	4699.003⌉	28.502	0.429		
22	4699.220⌋	26.219	0.270	41	7.99
22	4705.350	26.242	0.518	43	7.93
Si III 2	4552.620	19.018	0.283	64	6.00
2	4567.820	19.018	0.061	54	6.13
2	4574.760	19.018	-0.509	17	6.13

[1] blend of N II/O II (not used for the determination of ξ)

4.2. Analysis of the optical spectrum of ROA 5701

For the analysis of the CASPEC data of *ROA 5701* we used atomic data for C II (Yan et al., 1987), N II (Becker & Butler, 1989), O II (Bell et al., 1994) and Si III (Becker & Butler, 1990). Table 2 lists the results for individual lines. For C II we could only derive an upper limit, assuming an equivalent width of 10 mÅ for the C II line at 4267 Å. The spectrum synthesis resulted in abundances higher than those from the classical curve-of-growth analysis by about 0.1 dex for N II, O II, and Si III (cf. Table 5). Part of this offset is due to the fact that the spectrum synthesis has to use a "global continuum" for its fit (see also Sect. 2.3).

4.3. Iron abundances

Our main aim is to determine the iron abundances of both stars from the Fe III lines in the UV. We used the atomic data given by Ekberg (1993). The measured equivalent widths and the resulting abundances for both stars are listed in Table 3. The spectrum synthesis yields iron abundances about 0.2 dex lower than those obtained from the equivalent widths.

4.4. Error estimates

The iron abundances derived for *ROA 5701* and *Barnard 29* from different equivalent width measurements differ by up to 0.1 dex and 0.05 dex, respectively. The effects of differences in effective temperature, surface gravity, and microturbulent velocity are given in Table 4. To check the effects of using different line lists we also derived abundances using the line lists of Kurucz (1991, priv. comm., observed lines only). The derived mean abundances differed by about 0.05 dex from those given in Table 5. The errors given in Table 5 include those of Table 4 plus 0.05 dex (to account for possible errors in the line lists) and 0.1 dex resp. 0.05 dex in the iron abundances derived from W_λ (to account for errors in the equivalent widths measurements).

The stars we analyse are in a temperature-gravity range where NLTE effects start to play a rôle. Gies & Lambert (1992) and Kilian (1994) find that the NLTE abundances of C, N, O, and Si for B-type main sequence and supergiant stars are on average about 0.1 – 0.2 dex lower than the corresponding LTE abundances. As the

Table 3. Equivalent widths and abundances as derived from the GHRS spectra of *Barnard 29* and *ROA 5701*. We list the equivalent widths that were measured for a global continuum. Multiplet numbers are from Ekberg (1993).

Ion/ Multiplet	λ [Å]	χ [eV]	log gf	ROA 5701 W$_\lambda$ [mÅ]	ROA 5701 log ε	Barnard 29 W$_\lambda$ [mÅ]	Barnard 29 log ε
Fe III UV52	1866.315	7.869	-0.249	29	4.88		
UV52	1866.570	7.870	-0.770	25	5.33		
UV52	1869.837⌉	7.870	-2.134				
	1869.844⌋	7.870	-2.805				
	1869.927⌋	11.578	0.123			62	5.93
	1870.592	8.245	-1.665			6	5.58
	1871.336⌉	10.332	-0.646				
	1871.446⌋	10.332	-0.862	17	5.47		
	1872.211	11.144	0.243	21	5.09	54	5.64
	1873.549	10.317	-0.737			14	5.64
UV62	1878.003	8.639	0.312	50	4.80	54	4.87
	1878.547	8.238	-0.991			27	5.63
	1881.194	11.118	0.225	15	4.94	30	5.27
UV62	1882.050⌉	8.639	-0.082				
	1882.064⌋	8.650	-1.339			39	5.03
UV62	1884.597	8.656	-0.257	26	5.05	60	5.51
UV96	1885.965	10.308	-0.083	12	4.94	34	5.45
	1886.609⌉	8.656	-0.316				
UV52	1886.765⌋	7.867	0.336				
	1886.783⌋	11.144	-1.870	34	4.31	81	4.78
UV53	1887.212	7.867	-0.068	37	4.82	69	5.21
	1887.472⌉	7.870	-0.464				
UV52	1887.479	7.870	-1.541				
	1887.492⌋	7.869	-0.286	25	4.61	53	4.99
	1887.751⌉	14.170	0.484				
	1887.752⌋	7.870	-1.204	13	5.11	16	5.19
UV53	1889.463⌉	7.870	-0.302				
	1889.471⌋	7.870	-0.889	12	4.44	37	4.92
	1889.742	10.765	-0.141			22	5.39
UV52	1890.678	7.861	0.504	40	4.29		
UV53	1890.882⌉	7.870	-0.805				
	1890.882⌋	10.368	-2.528			28	5.36
UV52	1892.151⌉	7.867	-0.355				
UV96	1892.253	10.308	0.140				
	1892.348⌋	10.994	-0.409			197	6.08
	1892.882⌉	7.869	-1.205				
UV96	1892.896	10.308	-0.047				
	1893.111⌋	13.127	0.116	28	5.10	42	5.27
	1893.309	10.368	-0.387			12	5.21
UV83	1893.988	9.899	0.481	36	4.80	46	4.95
	1896.334	14.174	0.279			13	5.63
	1896.741⌉	10.225	-0.059				
UV83	1896.821⌋	9.897	0.514	51	4.84	105	5.44
	1897.385	9.899	-0.677			20	5.63
	1901.258⌉	10.305	-0.691				
	1901.383	10.225	-0.517				
	1901.394	10.211	-0.073				
UV96	1901.549⌋	10.368	-1.813	31	5.14	95	5.83
UV94	1902.098	10.308	0.118			36	5.28
	1902.411	10.215	-0.051			44	5.54
	1902.910	10.895	0.243			30	5.20
	1903.177⌉	10.308	-1.003				
	1903.263⌋	9.153	-0.547			49	5.70
	1904.265⌉	13.581	0.224				
	1904.384	13.127	-0.235				
	1904.412⌋	8.656	-0.274			58	5.37

Table 4. Error estimates

Star	Ion	$\Delta \log \epsilon$ from W_λ			$\Delta \log \epsilon$ from spectrum synthesis		
		± 1000 K	± 0.1 dex	± 5 km/s	± 1000 K	± 0.1 dex	± 5 km/s
ROA 5701	C II	± 0.08	∓ 0.03	∓ 0.01	± 0.03	∓ 0.03	± 0.05
	N II	± 0.00	∓ 0.00	∓ 0.01	± 0.02	∓ 0.01	∓ 0.01
	O II	∓ 0.12	± 0.04	∓ 0.04	∓ 0.13	± 0.01	∓ 0.02
	Si III	∓ 0.06	± 0.03	∓ 0.02	∓ 0.07	± 0.03	± 0.01
	Fe III	± 0.03	± 0.02	∓ 0.01	∓ 0.04	± 0.04	± 0.02
Barnard 29	Fe III	∓ 0.04	± 0.04	∓ 0.11	∓ 0.05	± 0.04	∓ 0.08

NLTE corrections shift the abundances of all elements in the same direction the relative abundance trends remain unchanged within our error bars.

Prompted by a remark from the referee Dr. P. Dufton we investigated whether the low iron abundances that we derived from UV lines of Fe III might be due to systematic errors. For this check we obtained 6 high resolution UV spectra of the normal main sequence B star γ Peg from the IUE final archive, which we coadded in order to increase the S/N. As line blending, continuum placement and incompleteness of atomic line lists are much more severe problems for solar metallicity B stars than for our (metal-poor) programme stars, we synthesized the spectral range in question using the entire Kurucz line list and varied the iron abundance. From the IUE data we get an iron abundance of $\log \epsilon_{Fe} = 6.95$[3]. This is at variance with the near solar value ($\log \epsilon_{Fe} = 7.56$, Pintado & Adelman, 1993) derived from the analysis of optical Fe III lines for this star, which we confirm from ESO CASPEC spectra. A similar discrepancy has been found by Grigsby et al. (1996) for the normal main sequence B star ι Her, for which the iron abundance from ultraviolet Fe II and Fe III lines was found to be more than 0.47 dex below the near solar value obtained from the analysis of optical lines. Grigsby et al. argue that the lower iron abundance derived from the UV lines is the correct one, as the abundances for both ions agree, whereas the previous optical analyses found differences between the two ions of up to 1.0 dex.

In summary the UV spectral analysis of normal B stars is currently so severely hampered by line crowding, continuum definition and incompleteness of atomic data that it is impossible to draw any clear cut conclusions on systematic abundance offsets for our metal poor programme stars, which are much less affected by these problems. We therefore do not apply any offsets to the iron abundances derived from the GHRS spectra.

5. Discussion

The results of our abundance analyses are given in Table 5, where we also give the results of Conlon et al. (1994) and Dixon & Hurwitz (1998) for *Barnard 29*. A comparison of

[3]   An error of 5% in the continuum definition results in an error of 0.2 dex in the iron abundance.
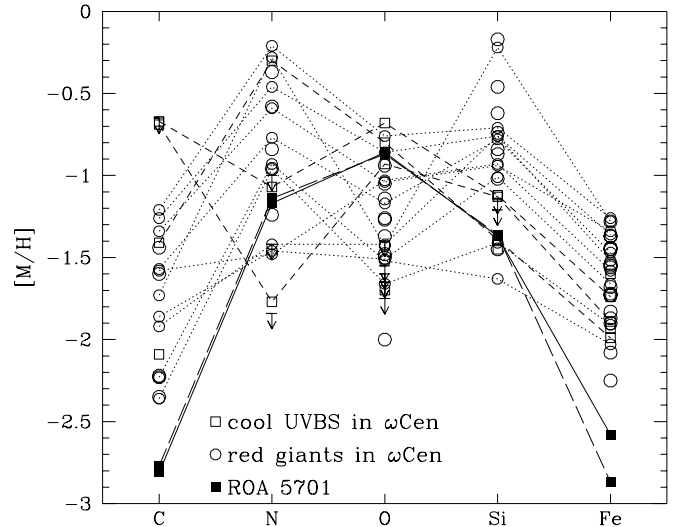
Fig. 2. The abundances derived for *Barnard 29* compared to those of red giant stars in M 13. The solid line connects the abundances derived for *Barnard 29* from curve-of-growth analyses. The dotted and short-dashed lines mark the abundances of the red giants taken from Smith et al. (1996) resp. Kraft et al. (1997).

our results with RGB and cooler UV bright stars (only in ω Cen) is presented in Figs. 2 and 3. The M 13 data in Fig. 2 are from Smith et al. (1996) and Kraft et al. (1997). The ω Cen data for the giants in Fig. 3 were collected from Paltoglou & Norris (1989), Brown et al. (1991), Brown & Wallerstein (1993), and Smith et al. (1995), the data for the cool UVBS are from Gonzalez & Wallerstein (1994). All abundances were adjusted to a solar iron abundance of $\log \epsilon_{Fe} = 7.50$.

As can be seen from Fig. 2 *Barnard 29* shows similar abundance trends (except for iron) as the giant stars observed in M 13. This abundance pattern is likely caused by deep mixing and dredge-up of CNO-processed material on the first RGB (Pilachowski et al., 1996). However, the iron abundance we found for *Barnard 29* is lower than the cluster value by 0.5 dex. This indicates that the atmosphere of *Barnard 29* has become iron depleted during the star's evolution, most likely by the gas-dust separation proposed by Bond (1991) and discussed by Napiwotzki et al. (1994), which is also favoured by Dixon & Hurwitz (1998) for *Barnard 29*. This scenario assumes that

Table 5. Abundances derived for *ROA 5701* and *Barnard 29*. $\log \epsilon$ gives the number abundance of the respective element with $\log \epsilon = \log (X/H) + 12$.

	ROA 5701					Barnard 29				remarks
$\log \epsilon_C$	$\log \epsilon_N$	$\log \epsilon_O$	$\log \epsilon_{Si}$	$\log \epsilon_{Fe}$	$\log \epsilon_C$	$\log \epsilon_N$	$\log \epsilon_O$	$\log \epsilon_{Si}$	$\log \epsilon_{Fe}$	
<5.78	6.83	7.93	6.08	4.89		7.30[1]	7.60[1]	6.30[1]	5.38	W_λ
±0.10	±0.05	±0.14	±0.09	±0.12		±0.11[1]	±0.20[1]	±0.27[1]	±0.14	
≤5.92	6.89	8.00	6.20	4.68	6.15[2]				5.21	spectrum synthesis
±0.08	±0.06	±0.14	±0.09	±0.08	±0.10[2]				±0.10	
8.58	8.05	8.93	7.55	7.50	8.58	8.05	8.93	7.55	7.50	solar values
[C/H]	[N/H]	[O/H]	[Si/H]	[Fe/H]	[C/H]	[N/H]	[O/H]	[Si/H]	[Fe/H]	
< −2.80	−1.22	−1.00	−1.47	−2.61		−0.75[1]	−1.33[1]	−1.25[1]	−2.12	W_λ
≤ −2.66	−1.16	−0.93	−1.35	−2.82	−2.33[2]				−2.29	spectrum synthesis

[1] Conlon et al. (1994)

[2] Dixon & Hurwitz (1998)
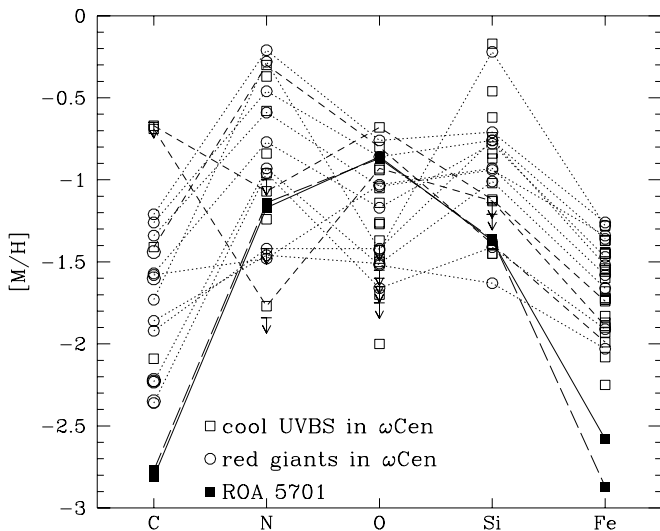
Fig. 3. The abundances derived for *ROA 5701* compared to those of other stars in ω Cen. The solid and long-dashed lines connect the abundances derived for *ROA 5701* from curve-of-growth and spectrum synthesis analysis, respectively. The short dashed lines mark the cool UV bright stars, the dotted lines connect the abundances of the red giants. For references see text.

the dust formed in the cool and extended atmospheres of AGB stars is selectively removed by radiation pressure, while the gas remains at the stellar surface. Since metals with high condensation temperatures (e.g. iron) preferentially condense into dust grains and elements with lower condensation temperatures remain in the gas phase, the remaining gas forms a iron-poor atmosphere. Mathis & Lamers (1992) discussed a single-star and a binary scenario, which can both result in a selective removal of dust at the end of the AGB stage.

The interpretation of the abundance pattern of *ROA 5701* is hampered by the complex patterns found in ω Cen stars in general (cf. Fig. 3). If we take as a metal-licity tracer the sum of C[4], N, and O abundances (which remains unchanged by CNO processing), we find that the original metallicity of *ROA 5701* is close to the median value determined for cluster stars (cf. Fig. 4). However, the iron abundance is 0.5 dex below the lowest value found for any RGB star plotted in Fig. 3. This points to an iron depletion similar to that detected in *Barnard 29*, which also shows a similar behaviour in Fig. 4.

In summary, the C, N, O, and Si abundances of *Barnard 29* and *ROA 5701* are in agreement with that of the respective cluster red giant stars. No dredge-up during the AGB phase is necessary to explain these abundance patterns, although a moderate third dredge-up cannot be ruled out from our data alone. However, our low iron abundances point towards a significant iron depletion, most probably caused by a gas-dust separation during the late AGB stages.

References

Becker S.R., Butler K., 1989, A&A 209, 244

Becker S.R., Butler K., 1990, A&A 235, 326

Bell K.L., Hibbert A., Stafford R.P., McLaughlin B.M., 1994, Physica Scripta 50, 343

Bergeron P., Saffer R.A., Liebert J., 1992, ApJ 394, 228

Bond H.E. 1991, in: *IAU Symp. No. 145*, eds. G. Michaud, A. Tutukov, p. 341

Brown J.A., Wallerstein G., Cunha K., Smith V.V., 1991, A&A 249, L13

Brown J.A., Wallerstein G., 1993, AJ 106, 133

Cacciari C., Caloi V., Castellani V., Fusi Pecci F., 1984, A&A 139, 258

[4] One should keep in mind that the upper limit for the C abundance was derived solely from the 4267 Å line, for which NLTE effects (Eber & Butler, 1988) can lead to abundances too low by up to 0.5 dex.
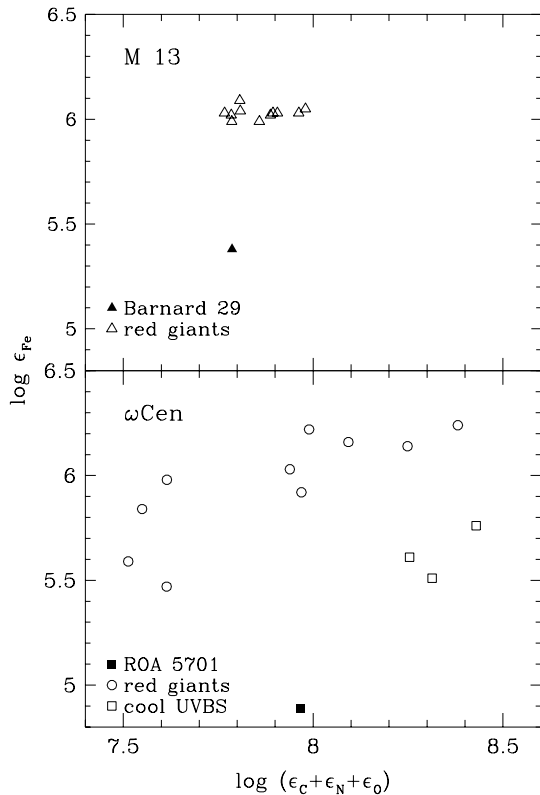
Fig. 4. Upper panel: The Fe abundances vs. the sum of CNO abundances for *Barnard 29* compared to those of red giants in M 13. For references see text. **Lower panel:** The Fe abundances vs. the sum of CNO abundances for *ROA 5701* compared to those of giants and cool UVBS in ω Cen. For references see text.

Conlon E.S. 1994, in *Hot Stars in the Galactic Halo*, eds. S. Adelman, A. Upgren, C.J. Adelman, CUP, p. 309

Conlon E.S., Dufton, P.L., Keenan, F.P. 1994, A&A 290, 897

de Boer K.S., 1987, in *The 2nd Conference on Faint Blue Stars*, eds. A.G.D. Philip, D.S. Hayes, J. Liebert, Davis Press, p. 95

Dixon W.V., Hurwitz M., 1998, ApJ 500, L29

Djorgovski S., 1993, in *Structure and Dynamics of Globular Clusters*, eds. S.G. Djorgovski & G. Meylan, ASP Conf. Ser. 50, p. 373

Dorman B., Rood R.T., O'Connell R.W., 1993, ApJ 419, 596

Eber F., Butler K., 1988, A&A 202, 153

Ekberg J.O., 1993, A&AS 101, 1

Gies D.R., Lambert D.L., 1992, ApJ 387, 673

Gonzalez G., Wallerstein G., 1994, AJ 108, 1325

Grigsby J.A., Mulliss C.L., Baer G.M., 1996, PASP 108, 953

Heber U., Hunger K., Jonas G., Kudritzki R.P., 1984, A&A 130, 119

Heber U., Werner K., Drilling J.S., 1988, A&A 194,223

Heber U., Dreizler S., Werner, K. 1993, Acta Astron. 43, 337

Iben, I.Jr., Renzini, A. 1984, Phys. Rep. 105, 329

Kraft R.P., Sneden C., Smith G.H., Shetrone M.D., Langer G.E., Pilachowski C.A., 1997, AJ 113, 279

Kilian J., 1994, A&A 282, 867

Kurucz R.L., 1992, IAU Symp. 149, 225

Mathis J.S., Lamers, H.J.G.L.M. 1992 A&A 259, L39

McCausland R.J.H., Conlon E.S., Dufton P.L., Keenan F.P. 1992, ApJ 394, 298

Napiwotzki R., Heber U., Köppen, J. 1994, A&A 292, 239

Norris J., 1974, ApJ 194, 109

Paltoglou G., Norris J.E., 1989, ApJ 336, 185

Pintado O.I., Adelman S.J., 1993, MNRAS 264, 63

Pilachowski C.A., Sneden C., Kraft R.P., Langer G.E., 1996, AJ 112, 545

Ponz D., Brinks E., 1986, ESO Messenger 43, 31

Renzini, A., Voli, M. 1981, A&A 94, 175

Saffer R.A., Bergeron P., Koester D., Liebert J., 1994, ApJ 432 351

Savage B.D., Mathis F.S., 1979, ARAA 17,73

Smith V.V., Cunha K., Lambert D.L., 1995, AJ 110, 2827

Smith G.H., Shetrone M.D., Bell R.A., Churchill C.W., Briley M.M., 1996, AJ 112, 1511

Sweigart A.V., Mengel J.G., Demarque P., 1974, A&A 30, 13

Vassiliadis E., Wood P.R. 1993, ApJ 413, 641

Yan Y., Taylor K.T., Seaton M.J., 1987, J. Phys. B 20, 6399

Zinn R.J., Newell E.B., Gibson J.B., 1972, A&A 18, 390